



1 Measurement report: Emissions of intermediate-volatility organic compounds from
2 vehicles under real-world driving conditions in an urban tunnel

3 Hua Fang^{1,2,4}, Xiaoqing Huang^{1,2,4}, Yanli Zhang^{1,2,3*}, Chenglei Pei^{1,4,5}, Zuzhao Huang⁶, Yujun Wang⁵,
4 Yanning Chen⁵, Jianhong Yan⁷, Jianqiang Zeng^{1,2,4}, Shaoxuan Xiao^{1,2,4}, Shilu Luo^{1,2,4}, Sheng Li^{1,2,4}, Jun
5 Wang^{1,2,4}, Ming Zhu^{1,2,4}, Xuwei Fu^{1,2,4}, Zhenfeng Wu^{1,2,4}, Runqi Zhang^{1,2,4}, Wei Song^{1,2}, Guohua
6 Zhang^{1,2}, Weiwei Hu^{1,2}, Mingjin Tang^{1,2}, Xiang Ding^{1,2}, Xinhui Bi^{1,2}, Xinming Wang^{1,2,3,4*}

7

8 ¹State Key Laboratory of Organic Geochemistry and Guangdong Key Laboratory of
9 Environmental Protection and Resources Utilization, Guangzhou Institute of Geochemistry,
10 Chinese Academy of Sciences, Guangzhou 510640, China

11 ²CAS Center for Excellence in Deep Earth Science, Guangzhou, 510640, China

12 ³Center for Excellence in Urban Atmospheric Environment, Institute of Urban Environment,
13 Chinese Academy of Sciences, Xiamen 361021, China

14 ⁴University of Chinese Academy of Sciences, Beijing 100049, China

15 ⁵Guangzhou Ecological and Environmental Monitoring Center of Guangdong Province,
16 Guangzhou 510060, China

17 ⁶Guangzhou Environmental Technology Center, Guangzhou 510180, China

18 ⁷Guangzhou Tunnel Development Company, Guangzhou 510133, China

19

20 *Correspondence to: Dr. Xinming Wang (e-mail: wangxm@gig.ac.cn) and Dr. Yanli Zhang (e-
21 mail: Zhang_yl86@gig.ac.cn)

22



23 **Abstract**

24 Intermediate-volatility organic compounds (IVOCs) emitted from vehicles are important
25 precursors to secondary organic aerosols (SOA) in urban areas, yet vehicular emission of
26 IVOCs, particularly from on-road fleets, is poorly understood. Here we initiated a field
27 campaign to collect IVOCs with sorption tubes at both the inlet and the outlet in a busy urban
28 tunnel (>30,000 vehicles per day) in south China for characterizing emissions of IVOCs from
29 on-road vehicles. The average emission factor of IVOCs (EF_{IVOCs}) was measured to be $16.77 \pm$
30 0.89 mg km^{-1} (Average $\pm 95\%$ C.I.) for diesel and gasoline vehicles in the fleets, and based on
31 linear regression the average EF_{IVOCs} was derived to be $62.79 \pm 18.37 \text{ mg km}^{-1}$ for diesel
32 vehicles and $13.95 \pm 1.13 \text{ mg km}^{-1}$ for gasoline vehicles. The EF_{IVOCs} for diesel vehicles from
33 this study was comparable to that reported previously for non-road engines without after-
34 treatment facilities, while the EF_{IVOCs} for gasoline vehicles from this study was much higher
35 than that recently tested for a China V gasoline vehicle. IVOCs from the on-road fleets did not
36 show significant correlation with the primary organic aerosol (POA) or total non-methane
37 hydrocarbons (NMHCs) as results from previous chassis dynamometer tests. Estimated SOA
38 production from the vehicular IVOCs and VOCs surpassed the POA by a factor of ~ 2.4 , and
39 IVOCs dominated over VOCs in estimated SOA production by a factor of ~ 7 , suggesting that
40 controlling IVOCs is of greater importance to modulate traffic-related OA in urban areas. The
41 results demonstrated that although on-road gasoline vehicles have much lower EF_{IVOCs} , they
42 contribute more IVOCs than on-road diesel vehicles due to its dominance in the on-road fleets.
43 However, due to greater diesel than gasoline fuel consumption in China, emission of IVOCs



- 44 from diesel engines would be much larger than that from gasoline engines, signaling the
- 45 overwhelming contribution of IVOC emissions by non-road diesel engines in China.



46 **1 Introduction**

47 Intermediate-volatility organic compounds (IVOCs) refer to organics with effective saturated
48 concentrations ranging from 10^3 to 10^6 $\mu\text{g m}^{-3}$, roughly corresponding to the volatility range of
49 C_{12} - C_{22} normal alkanes (n-alkanes) (Donahue et al., 2006; Zhao et al., 2014). Robinson et al.
50 (2007) have demonstrated that IVOCs, as the missing secondary organic aerosol (SOA)
51 precursors in many model studies, could efficiently narrow the gap between model predicted
52 and field observed SOA. Smog chamber studies involving individual IVOCs species, like
53 higher n-alkanes and 2-ring aromatics, have confirmed their significantly higher SOA formation
54 potentials (Chan et al., 2009; Presto et al., 2010; Liu et al., 2015). In addition, recent model
55 simulations including IVOCs as SOA precursors revealed that 30% ~ 80% of ambient SOA
56 could be explained by IVOCs (Ots et al., 2016; Zhao et al., 2016; Yang et al., 2019; Lu et al.,
57 2020; Huang et al., 2020). However, due to lack of direct measurements, these model
58 simulations used the ratios of IVOCs to other species like primary organic aerosol (POA) or
59 non-methane hydrocarbons (NMHCs) to estimate IVOCs emissions.

60 Vehicular emission is an important anthropogenic source of IVOCs especially in urban
61 environments (Tkacik et al., 2014; Jathar et al., 2014; Cross et al., 2015; Zhao et al., 2015, 2016;
62 Ots et al., 2016). IVOCs could account for ~ 60% of non-methane hydrocarbons (NMHCs)
63 from diesel vehicles and 4 – 17% from gasoline vehicles, explaining a dominant portion of
64 estimated SOA mass from diesel and gasoline exhaust (Zhao et al., 2015, 2016). Previous
65 chamber simulations on SOA formation from vehicle exhaust revealed that traditional volatile
66 organic compounds (VOCs) could not explain the formed SOA, and IVOCs instead might
67 dominate the SOA productions (Deng et al., 2020; Zhang et al., 2020). In megacities like
68 London, diesel-emitted IVOCs alone could contribute ~ 30% SOA formed in ambient air (Ots



69 et al., 2016). Therefore, for the control of fine particle pollution in urban areas, it is necessary
70 to compile and upgrade emission inventories for IVOCs, and more works are needed to
71 characterize their emissions from on-road vehicles.

72 Although previous chassis dynamometer tests used limited numbers of vehicles to characterize
73 IVOCs emission (Zhao et al., 2015, 2016; Tang et al., 2021), the results obtained from the tests
74 were widely applied to recent models and emission inventories (Liu et al., 2017; Lu et al., 2018;
75 Wu et al., 2019; Huang et al., 2020). However, driving conditions were recently found to
76 significantly influence vehicular IVOCs emissions (Drozd et al., 2018; Tang et al., 2021),
77 highlighting the importance of conducting on-road measurements of vehicle-emitted IVOCs
78 under real-world driving condition, which could further narrow the uncertainty of vehicular
79 IVOCs estimates in models and emission inventories. Tunnel test is a widely used method to
80 characterize vehicle emissions in light of its advantage in capturing real-world emissions with
81 a large number of driving vehicles. The emissions of $PM_{2.5}$, carbonaceous aerosols, VOCs, NO_x,
82 and NH₃ from on-road vehicles have been widely studied based on tunnel tests (Liu et al., 2014;
83 Zhang et al., 2016, 2017, 2018). However, to the best of knowledge, till present no reports are
84 available about vehicular emission factors of IVOCs through tunnel tests.

85 In China, the number of on-road vehicles reached 348 million in 2019, more than double that
86 in 2009 (<http://www.mee.gov.cn/hjzl/sthjzk/ydyhjgl/>). However, emissions of IVOCs from
87 mobile sources in China are much understudied. Only very recently, Tang et al. (2021) tested
88 emission of IVOCs from a China V light-duty gasoline vehicle. For this reason, IVOC emission
89 factors derived from vehicle tests in the US have been used to update China's emission
90 inventories with the inclusion of IVOCs (Liu et al., 2017). It is unknown whether the borrowed



91 emission factors could well reflect the vehicular emissions of IVOCs in China. On the other
92 hand, although China has made great achievements in combating air pollution in recent years,
93 fine particle pollution is still an air quality problem in many of China's cities (Wang et al., 2020).
94 As organic matters are often the most abundant components in PM_{2.5} and SOA pollution is
95 increasingly standing out with the intensified primary emission control (Guo et al., 2020),
96 understanding IVOC emissions from on-road vehicles is of great importance given that vehicle-
97 emitted IVOCs contribute greatly to urban SOA formation (Gentner et al., 2012; Wu et al., 2019;
98 Huang et al., 2020).

99 In this study, the emissions of IVOCs from on-road vehicles under real-world driving conditions
100 were characterized through tests in an urban tunnel in Guangzhou, a megacity in south China.
101 The study aims to: 1) investigate chemical compositions and volatility of IVOCs from on-road
102 driving vehicles; 2) obtain average IVOC emission factors for on-road fleet based on tests in
103 the tunnel; 3) retrieve average IVOC emission factors for gasoline- and diesel-fueled vehicles
104 by regression analysis, taking advantage of a large number of vehicles (>30,000 per day)
105 passing the tunnel; 4) compare the SOA formation potential of vehicle-emitted IVOCs to that
106 of vehicle-emitted VOCs measured in the same campaign.

107 **2. Methodology**

108 **2.1 Field sampling**

109 Sampling campaign was concurrently conducted both at the inlet and at the outlet of the
110 Zhujiang tunnel (23 °6' N, 113 °14' E), which is located in urban Guangzhou, South China (Fig.
111 S1), on three weekdays (October 14th-16th, 2019) and two weekend days (October 13th and



112 October 19th, 2019). Detailed description of the Zhujiang tunnel could be found in our previous
113 studies (Liu et al., 2014; Zhang et al., 2016, 2017, 2018). IVOCs were collected by a sorption
114 tube (Tenax TA/ Carbograph 5TD, Marks International Ltd, UK) using an automatic sampler
115 (JEC921, Jectec Science and Technology, Co., Ltd, Beijing, China). A Teflon filter was installed
116 before the tube to remove particles in the air flow. The sampling flow rate was set at 0.6 L min⁻¹
117 and hourly samples were collected from 5:00 am to 24:00 pm on each sampling day. In order
118 to compare SOA productions from IVOCs and VOCs, hourly VOCs samples were collected on
119 13th October 2019 with stainless-steel canisters at a flow rate of 66.7 mL min⁻¹ using a Model
120 910 Pressurized Canister Sampler (Xonteck, Inc., CA, USA). 2-hour quartz filter samples were
121 also collected by a high-volume PM_{2.5} sampler (Thermo Electron, Inc., USA) at the outlet and
122 inlet sampling sites from 13th October to 19th October. Trace gases were measured by online
123 analyzers (CO, Model 48i, Thermo Electron Inc., USA; NO_x, Model 42i, Thermo Electron Inc.,
124 USA). A video camera was installed at the inlet to record the vehicle flow during the campaign.
125 After sampling, the videotapes were used to count the passing vehicles and classify the vehicle
126 types.

127 **2.2 Laboratory analysis**

128 Sampled sorption tubes were analyzed by a thermal desorption (TD) system (TD-100, Markes
129 International Ltd, UK) coupled to a gas chromatography / mass selective detector (GC/MSD;
130 Agilent, 7890 GC/5975 MSD, USA) with a capillary column (Agilent, HP-5MS, 30 m × 0.25
131 mm × 0.25 μm). Deuterated standards (C₁₂-d₂₆, C₁₆-d₃₄, C₂₀-d₄₂, naphthalene-d₈, acenaphthene-
132 d₁₀ and phenanthrene-d₁₀) were injected into the sorption tubes to determine their recoveries
133 before analysis. The sampled sorption tubes and field blanks were thermally desorbed at 320 °C



134 for 20 min, and the desorbed compounds were carried by high purity helium into a cryogenic
135 trap at $-10\text{ }^{\circ}\text{C}$, and then the trap was rapidly heated to transfer them into the GC/MSD system.
136 The initial temperature of GC oven was set at $65\text{ }^{\circ}\text{C}$, held for 2 min, then increased to $290\text{ }^{\circ}\text{C}$
137 at $5\text{ }^{\circ}\text{C min}^{-1}$ and kept at $290\text{ }^{\circ}\text{C}$ for 20 min. The MSD was used in the SCAN mode with an
138 electron impacting ionization at 70 eV.
139 Individual speciated IVOCs were quantified with the calibration curves by using authentic
140 standards. The total IVOCs mass was determined using the approach developed by Zhao et al.
141 (2014, 2015, 2016) and the detailed description was provided in the supporting information
142 (Text S1). Briefly, the total ion chromatogram (TIC) of IVOCs was divided into 11 bins based
143 on the retention time of C_{12} - C_{22} n-alkanes. Each bin centered on the retention time of n-alkane.
144 The start time and end time of the bin was determined by the average retention time of two
145 successive n-alkanes. For example, the start time of Bin16 (B16) was calculated as the average
146 retention time of n- C_{15} and n- C_{16} , and the end time of B16 as the average retention time of n-
147 C_{16} and n- C_{17} . The IVOCs mass in each bin was quantified by the response factor of n-alkane
148 in the same bin. The total IVOCs mass was the sum of IVOCs mass determined in 11 bins. The
149 mass of unresolved complex mixtures of IVOCs (UCM-IVOCs) was determined by the
150 difference between the total IVOCs and speciated IVOCs in each bin. The UCM-IVOCs were
151 further classified into unspciated branch alkanes (b-alkanes) and cyclic compounds (Zhao et
152 al., 2014) (Text S1). The analysis of VOCs can be found elsewhere (Zhang et al., 2018). The
153 POA emission was estimated as 1.2 times of organic carbon that measured in quartz filter
154 samples (Zhao et al., 2015), which were analyzed by an OC/EC analyzer (DRI Model 2015,
155 Nevada, USA) (Li et al., 2018).



156 **2.3 Quality assurance and quality control (QA/QC)**

157 Before their use for field sampling, sorption tubes were conditioned at 320 °C for 2 hours at
158 oxygen-free nitrogen flow and then sealed at both ends with brass storage caps fitted with PTFE
159 ferrules. About 15% of conditioned tubes were selected randomly to be analyzed in the same
160 way as normal samples to check if any targeted species existed in the tubes. The batch of
161 sorption tubes were certified as clean if speciated IVOCs were not found or presented in levels
162 below the method detection limits (MDLs). Before and after sampling, the flow rates of
163 samplers were calibrated by a soap-membrane flowmeter (Gilian Gilibrator-2, Sensidyne,
164 USA). During the sampling, ten field blanks (five at the inlet and five at the outlet) were
165 collected by installing a sorption tube onto the sampler each day but with pump off at both the
166 inlet and the outlet. The speciated IVOCs were not detected or presented in levels below their
167 MDLs in the blanks. MDLs for all the speciated IVOCs, including n-alkanes and polycyclic
168 aromatic hydrocarbons (PAHs), were below 8 ng m⁻³, such as 5.8 ng m⁻³ for n-C₁₂, 5.9 ng m⁻³
169 for n-C₁₆ and 4.7 ng m⁻³ for n-C₂₂. To check if any breakthrough occurs during the sampling,
170 prior to the field campaign two sorption tubes were connected in series to sample at the tunnel
171 outlet station in the same way. IVOCs detected in the second tube only accounted for 2.6 ± 1.4%
172 of the total in the two tubes, indicating no breakthrough during the sampling. To check the
173 recoveries during thermo-desorption, selected sampled sorption tubes were analyzed twice by
174 the TD-GC/MS system, and the desorption recoveries, calculated as the percentage of IVOCs
175 in first analysis, were 96.7 ± 3.2% on average. Duplicated samples revealed less than 15%
176 differences for all the speciated IVOCs.

177 **2.4 Calculation of IVOCs emission factor**



178 The vehicular EF of IVOCs can be calculated by following equation (Pierson et al., 1983; Zhang
179 et al., 2016, 2017, 2018):

$$180 \quad EF = \frac{\Delta C \times V_{air} \times T \times A}{N \times l} \quad (1)$$

181 where EF ($\text{mg km}^{-1} \text{veh}^{-1}$) is the fleet-average emission factor of given species during the time
182 interval T (1 h in this study); ΔC (mg m^{-3}) is the inlet-outlet incremental concentration of IVOCs;
183 V_{air} (m s^{-1}) is wind speed parallel to the tunnel measured by a 3-D sonic anemometer (Campbell,
184 Inc.); A (m^2) is the cross sectional area of the tunnel; N is the number of vehicles travelling
185 through the tunnel during the time interval T; l (km) is the distance between the outlet and the
186 inlet.

187 3. Results and discussions

188 3.1 Emission factors and compositions of IVOCs

189 Fig. 1 shows diurnal variations of vehicle numbers and vehicular IVOCs emission factors
190 (EF_{IVOCs}) during the campaign. Traffic flow in the tunnel varied 571-2263 vehicles per hour
191 during the campaign, and gasoline vehicles (GVs) dominated the vehicle fleets with a share of
192 76.3%, diesel vehicles (DVs) only accounted for 4.0%, and other types of vehicles, including
193 liquefied petroleum gas vehicles (LPGVs) and electrical vehicles (EVs), had a percentage of
194 18.7% (Fig. S2). As LPGVs and EVs are considered to have no IVOCs emissions (Stewart et
195 al., 2021), only GV and DVs are responsible for the inlet-outlet incremental concentrations of
196 IVOCs. Based on above equation (1), average EF_{IVOCs} for GV and DVs in the vehicle fleets
197 ranged from $13.29 \pm 5.08 \text{ mg km}^{-1} \text{veh}^{-1}$ to $21.40 \pm 5.01 \text{ mg km}^{-1} \text{veh}^{-1}$, with an average of 16.77
198 $\pm 0.89 \text{ mg km}^{-1} \text{veh}^{-1}$ (Average $\pm 95\%$ C.I.) (Fig. 1). The average EF_{IVOCs} for DVs and GV
199 could be further derived through linear regression as below (Ho et al., 2007; Kramer et al.,



200 2020):

$$201 \quad EF_{IVOCs} = EF_{DV} \times \alpha + EF_{GV} \times (1 - \alpha) \quad (2)$$

202 where EF_{IVOCs} represents the fleet-average emission factor measured during a time interval;

203 EF_{DV} and EF_{GV} are the average EF_{IVOCs} for DVs and GVs, respectively; α is the fraction of

204 DVs in the total IVOCs-emitting diesel and GVs traveling through the tunnel. Based on the

205 regression results (Fig. S3), the average EF_{IVOCs} for DVs ($62.79 \pm 18.37 \text{ mg km}^{-1}\text{veh}^{-1}$) was ~

206 4.5 times that for GVs ($13.95 \pm 1.13 \text{ mg km}^{-1} \text{veh}^{-1}$).

207 The mileage-based EF can be converted to fuel-based EF with the fuel density and fuel

208 efficiency (Text S2) (Zhang et al., 2016). Thus, we could obtain an average fuel-based EF_{IVOCs}

209 of $239.5 \pm 19.5 \text{ mg kg}^{-1}$ for GVs and $984.9 \pm 288.2 \text{ mg kg}^{-1}$ for DVs. Zhao et al. (2015, 2016)

210 measured IVOCs emissions from DVs and GVs in the US by the dynamometer tests. As shown

211 in Fig. 2, the average EF_{IVOCs} for DVs measured in our study was significantly lower than that

212 for DVs without any diesel particulate filter (DPF) in the US, but over 4 times higher than that

213 with DPF. It is worth noting that the EF_{IVOCs} for DVs from this study was comparable to that

214 for ships and non-road construction machineries (NRCMs) with diesel-fueled engines in China

215 (Fig. 2) (Huang et al., 2018; Qi et al., 2019). As a matter of fact, China III or lower emission

216 standard DVs accounted for ~ 40% of China's total in-use DVs in 2019

217 (<http://www.mee.gov.cn/>), and like the non-road engines, they are not equipped with any after-

218 treatment facilities. Although the after-treatment systems are installed in the China IV and

219 China V DVs, their working performance might be not so satisfactory (Wu et al., 2017). This

220 may explain why the DVs in this study had IVOCs-EFs comparable to non-road engines. The

221 EF_{IVOCs} for GVs from this study fell into the ranges of that for GVs in the US, but was at the



222 high-end of the tested values (Fig. 2). A recent study revealed a significantly lower EF_{IVOCs} of
223 83.7 mg kg^{-1} for a China V gasoline vehicle (Tang et al., 2021), implying that upgrading the
224 emission standard could help reduce emissions of IVOCs from GVs, as China IV and China III
225 GVs still share a much larger portion than the China V and VI ones in the on-road fleets
226 (<http://www.mee.gov.cn/>).

227 Fig. 3 shows the EFs and compositions of the vehicular IVOCs in each retention-time based
228 bin (Table S1). Similar to previous studies (Zhao et al., 2015, 2016; Huang et al., 2018; Qi et
229 al., 2019; Tang et al., 2021), the unspeciatiated cyclic compounds dominated the IVOCs,
230 accounting for $59.07 \pm 1.06\%$, followed by unspeciatiated b-alkanes ($25.27 \pm 0.75\%$) and
231 speciatiated IVOCs ($15.66 \pm 0.60\%$). The speciatiated IVOCs consist of n-alkanes, b-alkanes and
232 PAHs. Naphthalene dominated the quantified PAHs, accounting for $56.82 \pm 1.21\%$ of total
233 PAHs emissions. The distribution of IVOCs in retention-time based bins presented a significant
234 decreasing trend with bin numbers. Previous studies have reported that more than 50% of
235 IVOCs concentrated in higher-volatility bins like B12, B13 and B14 in gasoline exhaust while
236 much broader volatility distributions were found in diesel exhaust (Zhao et al., 2015, 2016;
237 Tang et al., 2021). The IVOCs in B12 measured in this study was also the most abundant as the
238 GVs previously tested in the US (Fig. S4). This was reasonable since the GVs dominated the
239 vehicle fleets during our tunnel experiments (Fig. S2). As shown in Fig. S5, the IVOCs
240 determined in each volatility bin well correlated with those in the volatility bins close to them,
241 and the total IVOCs have stronger correlations with IVOCs in the higher-volatility bins like
242 B12, B13 and B14. In addition, the n-alkanes, as displayed in Table S2, were found to be
243 significantly correlated to the total IVOCs that determined in the same volatility bin except for



244 B20 and n-C₂₀. The mass ratios of IVOCs in each bin to the n-alkane in the same bin ranges
245 9.0-15.8 (Table S2). As n-alkanes are more easily and routinely quantified, the relationships of
246 IVOCs and n-alkanes in each volatility bin might be used to estimate total IVOCs from on-road
247 vehicles. However, vehicles types should be taken into consideration when using these ratios,
248 as the results obtained here were based on a fleet dominated by GVs.

249 **3.2 Relationships of IVOCs with other species**

250 Emissions of IVOCs from vehicles are often estimated by assuming a ratio of IVOCs to other
251 species such as POA or NMHCs (Shrivastava et al., 2008; Pye et al., 2010; Gentner et al., 2012;
252 Murphy et al., 2017; Wu et al., 2019). However, these ratios might be highly variable with fuel
253 types, operation conditions and engine performance (Lu et al., 2018). As demonstrated in Fig.
254 S6 (a) and (b), IVOCs correlated well with NO_x ($R = 0.63$, $p < 0.05$) and CO ($R = 0.58$, $p <$
255 0.05), with an average IVOCs-to-NO_x ratio of 0.039 ± 0.004 and an average IVOCs-to-CO
256 ratio of 0.033 ± 0.015 . The measured IVOCs-to-POA ratio was 3.35 ± 1.79 (Fig. S6 (c)),
257 comparable to that of 3.0 ± 0.9 for GVs previously measured in dynamometer tests simulating
258 arterial and freeway cycles, but much higher than that of 1.5 previously used for estimating
259 vehicle emissions in models (Robinson et al., 2007; Hodzic et al., 2010). As shown in Fig. S6
260 (d), the average IVOCs-to-NMHCs ratio measured in this study was 0.36 ± 0.09 , lower than
261 that previously measured for diesel vehicle exhaust (0.6 ± 0.1) (Zhao et al., 2015), but higher
262 than that previously measured for gasoline vehicle exhaust (< 0.2) (Zhao et al., 2016; Tang et
263 al., 2021). It is worth noting that the IVOCs did not present significant correlations with POA
264 or NMHCs from this study for on-road vehicle fleets (Fig. S6 (c) and (d)). This would cast
265 uncertainty over the emission estimates of IVOCs based on their ratios to POA or NMHCs.



266 3.3 Estimated SOA production from IVOCs

267 SOA formation potentials of IVOCs from on-road vehicle fleet as measured in this tunnel study
268 can be estimated as:

$$269 \quad SOA_{FP} = \sum EF_i \times Y_i \quad (3)$$

270 where SOA_{FP} is the SOA formation potential from the gaseous precursors; EF_i represents the
271 emission factor of precursor i and Y_i is the SOA yield of precursor i under high-NO_x at OA
272 concentration of 20 $\mu\text{g m}^{-3}$ (Zhao et al., 2015; Huang et al., 2018; Qi et al., 2019; Tang et al.,
273 2021) (Table S3). As shown in Fig. 4, the SOA formation potentials from vehicular VOCs and
274 IVOCs totalled $8.24 \pm 0.68 \text{ mg km}^{-1}$. The SOA-to-POA ratio was 2.41 ± 1.45 , which was
275 comparable to that of GVs tested in China (1.8-4.4) (Tang et al., 2021), and that of GVs (3.6)
276 (Zhao et al., 2016) and high-speed DVs (3.2 ± 1.7) without DPF in the US (Zhao et al., 2015).
277 Our previous chamber studies simulating SOA formation from vehicles exhaust revealed the
278 SOA-to-POA ratios of 2.0 for DVs and 3.8 for GVs when cruising at 40 km h^{-1} (Deng et al.,
279 2020; Zhang et al., 2020), which is near the average driving speed of vehicles in the tunnel.
280 Among the vehicle-emitted SOA precursors, similar to previous studies (Zhao et al., 2015, 2016;
281 Huang et al., 2018; Qi et al., 2019; Tang et al., 2021), IVOCs produced significantly higher
282 SOA ($7.19 \pm 0.62 \text{ mg km}^{-1}$), ~ 7 times that from traditional VOCs ($1.04 \pm 0.30 \text{ mg km}^{-1}$).
283 Previous smog chamber studies found that SOA formed during photoaging of vehicle exhaust
284 could not be explained by traditional VOCs especially for vehicles cruising at higher speeds
285 (Robinson et al., 2007; Deng et al., 2020; Zhang et al., 2020). If this $SOA_{IVOCs\text{-to-}SOA_{VOCs}}$ ratio
286 of 7 from this study is used to re-estimate the SOA formation from exhaust for vehicles cruising
287 at 40 km h^{-1} in our previous chamber studies (Deng et al., 2020; Zhang et al., 2020), the VOCs



288 plus IVOCs precursors could explain 91% – 98% SOA formed for GVs and 31.2% – 48.2%
289 SOA formed for DVs. Zhao et al. (2015, 2016) reported significant higher $SOA_{IVOCs-to-}$
290 SOA_{VOCs} ratio for diesel vehicle exhaust than gasoline vehicle exhaust. Thus, $SOA_{IVOCs-to-}$
291 SOA_{VOCs} ratio of 7 obtained in a tunnel dominated by GVs would underestimate SOA_{IVOCs} from
292 DVs, consistent with higher NMHCs to IVOCs ratios in gasoline exhaust than in diesel exhaust
293 (Zhao et al., 2015, 2016; Huang et al., 2018; Qi et al., 2019; Tang et al., 2021). Overall, the
294 observed vehicular IVOCs as SOA precursors can help achieve mass closure between predicted
295 and measured SOA.

296 **4. Conclusions and implications**

297 Organic aerosol (OA), primary or secondary, accounts for a large fraction of particle matters
298 (Zhang et al., 2007; Jimenez et al., 2009). On-road vehicles could be an important source of
299 OA especially in urban environment (Gentner et al., 2017). Similar to previous smog chamber
300 simulation results about SOA formed from photochemical aging of vehicle exhaust (Deng et
301 al., 2020; Zhang et al., 2020), our tunnel test also demonstrated that estimated SOA surpassed
302 the POA emission. In addition, IVOCs was found to dominate over traditional VOCs in SOA
303 formation potentials by a factor of ~ 7 , implying that reducing vehicle-emitted IVOCs is of
304 greater importance to modulate SOA for further reducing fine particle pollution particularly in
305 urban areas. As for the ratios of IVOCs to other primary species, our tunnel tests for on-road
306 fleet revealed complex and different results when compared to that from previous chassis
307 dynamometer tests, implying that cautions should be taken when applying the ratios from
308 chassis dynamometer tests to estimate real-world traffic emissions, or applying the ratios in the
309 US to estimate the emissions in China or other regions. As IVOCs is not considered in normal



310 vehicle emission tests, more field works characterizing real-world vehicular emissions of
311 IVOCs are needed to further constrain these ratios.

312 EF_{IVOCs} for the GV-dominated fleets from our tunnel test, or EF_{IVOCs} for GVs derived from
313 regression, was much higher than that from a recent chassis test for a China V gasoline vehicle
314 (Tang et al., 2021), suggesting that stricter emission standards might help reduce emissions of
315 IVOCs from GVs. Meanwhile, the EF_{IVOCs} for on-road DVs was comparable to that for non-
316 road engines without any after-treatments (Huang et al., 2018; Qi et al., 2019), suggesting that
317 facilitating the installation of after-treatment devices with stricter emission standards or
318 improving the performance of existing after-treatment devices are crucial to lower IVOC
319 emissions from DVs, which have much bigger EF_{IVOCs} than GVs.

320 Based on the regression-derived average EF_{IVOCs} for GVs and DVs and the camera-recorded
321 fleet compositions, we could estimate that ~ 81% of IVOCs by vehicles travelling through the
322 tunnel were coming from GVs and only ~ 19% were from DVs. This is reasonable since DVs
323 have bigger EF_{IVOCs} and however much lower proportions in the fleets. These percentages may
324 underestimate the contribution to IVOCs by on-road DVs in regional or national scales since
325 DVs travel less in core urban areas due to traffic restriction rules in China. Differently, in an
326 updated emission inventory of vehicular IVOCs in China (Liu et al., 2017) based on EF_{IVOCs}
327 tested in the US, emission of IVOCs from DVs (145.07 Gg) was about 2.6 times that from GVs
328 (55.30 Gg) in China in 2015. However, the ratio of DV- EF_{IVOCs} to GV- EF_{IVOCs} used in the study
329 (Liu et al., 2017) on average was much higher than that of ~ 4.5 from this study for on-road
330 vehicles. Using the EF_{IVOCs} from tests in the US might underestimate IVOCs emissions from
331 GVs but overestimate that from DVs in China. As an example, EF_{IVOCs} of 83.7 mg kg⁻¹ reported



332 very recently for a China V gasoline vehicle (Tang et al., 2021) was still much higher than the
333 maximum EF_{IVOCs} (47.15 mg kg^{-1}) they adopted for China V GVs, and the EF_{IVOCs} used for
334 China III and China IV DVs were however significantly larger than that from our tunnel tests
335 (Fig. 2) for on-road DVs (mostly China III and China IV) (Liu et al., 2017). In 2019 the gasoline
336 and diesel fuel consumptions in China were $1.20 \times 10^2 \text{ Tg}$ and $1.50 \times 10^2 \text{ Tg}$, respectively
337 (<http://www.mee.gov.cn/hjzl/sthjzk/ydyhjgl/>). Since that gasoline is mostly used for on-road
338 vehicles while diesel may be used for both on-road and non-road engines, and that EF_{IVOCs} for
339 on-road diesels are comparable to the non-road diesel engines (Huang et al., 2018; Qi et al.,
340 2019), we could use the fuel-based EF_{IVOCs} converted from our study to roughly estimate IVOCs
341 from diesel and gasoline combustion. This way estimated emission of IVOCs from diesel
342 engines (147.74 Gg) was about 5 times that from gasoline engines (28.74 Gg) in China in 2019.
343 In comparison of previous study (Liu et al., 2017), this result implies large uncertainties or even
344 inconsistencies about China's vehicular IVOC emission estimates. Moreover, as diesel vehicle
345 shares less than 10% among China's motor vehicles and a substantial part of diesel fuel is
346 consumed by non-road engines, the diesel-related IVOCs may largely come overwhelmingly
347 from non-road engines instead of on-road DVs, signaling the increasingly important role of
348 non-road engines as sources of IVOCs with the progress in on-road vehicles emission control.



349 **Data availability.** The dataset for this paper is available upon request from the corresponding
350 author (wangxm@gig.ac.cn)

351 **Competing interests.** The authors declare no competing financial interest.

352 **Author Contributions.** X.W. and Y.Z. designed the campaign and provided the funding
353 supports. H.F. and H.X. analyzed the samples. H.F. wrote the paper. G.Z., W.H., M.T., X.D.,
354 and X.B. provided suggestions for this paper. X.W. revised and edited the paper. The others in
355 author list conducted the field work.

356 **Acknowledgements.**

357 This work was supported by funded by Natural Science Foundation of China
358 (41530641/41961144029), the National Key Research and Development Program
359 (2016YFC0202204/2017YFC0212802), the Chinese Academy of Sciences (QYZDJ-SSW-
360 DQC032), and Department of Science and Technology of Guangdong Province
361 (2017B030314057/2017BT01Z134/2019B121205006).



362 **References**

- 363 Chan, A. W. H., Kautzman, K. E., Chhabra, P. S., Surratt, J. D., Chan, M. N., Crouse, J. D.,
364 Kürten, A., Wennberg, P. O., Flagan, R. C., and Seinfeld, J. H.: Secondary organic aerosol
365 formation from photooxidation of naphthalene and alkylnaphthalenes: implications for
366 oxidation of intermediate volatility organic compounds (IVOCs). *Atmos. Chem. Phys.*, 9,
367 3049-3060, <https://doi.org/10.5194/acp-9-3049-2009>, 2009.
- 368 Cross, E. S., Sappok, A., Wong, V., and Kroll, J. H.: Load-dependent emission factors and
369 chemical characteristics of IVOCs from a medium-duty diesel engine. *Environ. Sci.*
370 *Technol.*, 49, 13483-13491, <https://doi.org/10.1021/acs.est.5b03954>, 2015.
- 371 Deng, W., Fang, Z., Wang, Z. Y., Zhu, M., Zhang, Y. L., Tang, M. J., Song, W., Lowther, S.,
372 Huang, Z. H., Jones, K., Peng, P. A., and Wang, X. M.: Primary emissions and secondary
373 organic aerosol formation from in-use diesel vehicle exhaust: comparison between idling
374 and cruise mode. *Sci. Total Environ.*, 699, 134357,
375 <https://doi.org/10.1016/j.scitotenv.2019.134357>, 2020.
- 376 Donahue, N. M., Robinson, A. L., Stanier, C. O., and Pandis, S. N.: Coupled partitioning,
377 dilution, and chemical aging of semivolatile organics. *Environ. Sci. Technol.*, 40, 2635-43,
378 <https://doi.org/10.1021/es052297c>, 2006.
- 379 Drozd, G. T., Zhao, Y. L., Saliba, G., Frodin, B., Maddox, C., Oliver Chang, M. C., Maldonado,
380 H., Sardar, S., Weber, R. J., Robinson, A. L., and Goldstein, A. H.: Detailed speciation of
381 intermediate volatility and semivolatile organic compound emissions from gasoline
382 vehicles: effects of cold-starts and implications for secondary organic aerosol formation.
383 *Environ. Sci. Technol.*, 53, 1706-1714. <https://doi.org/10.1021/acs.est.8b05600>, 2018.



384 Gentner, D. R., Isaacman, G., Worton, D. R., Chan, A. W. H., Dallmann, T. R., Davis, L., Liu,
385 S., Day, D. A., Russell, L. M., Wilson, K. R., Weber, R., Guha, A., Harley, R. A., and
386 Goldstein, A. H.: Elucidating secondary organic aerosol from diesel and gasoline vehicles
387 through detailed characterization of organic carbon emissions. *Proc. Natl. Acad. Sci. U. S.*
388 *A.*, 109, 18318–18323, <https://doi.org/10.1073/pnas.1212272109>, 2012.

389 Gentner, D. R., Jathar, S. H., Gordon, T. D., Bahreini, R., Day, D. A., El Haddad, I., Hays, P.
390 L., Pieber, S. M., Platt, S. M., de Gouw, J., Goldstein, A. H., Harley, R. A., Jimenez, J. L.,
391 Prévôt, A. S. H., and Robinson, A. L.: Review of urban secondary organic aerosol
392 formation from gasoline and diesel motor vehicle emissions. *Environ. Sci. Technol.*, 51,
393 1074-1093, <https://doi.org/10.1021/acs.est.6b04509>, 2017.

394 Guo, J. C., Zhou, S. Z., Cai, M. F., Zhao, J., Song, W., Zhao, W. X., Hu, W. W., Sun, Y. L., He,
395 Y., Yang, C. Q., Xu, X. Z., Zhang, Z. S., Cheng, P., Fan, Q., Hang, J., Fan, S. J., Wang, X.
396 M., and Wang, X. M.: Characterization of submicron particles by time-of-flight aerosol
397 chemical speciation monitor (ToF-ACSM) during wintertime: aerosol composition,
398 sources, and chemical processes in Guangzhou, China. *Atmos. Chem. Phys.*, 20, 7595-
399 7615, <https://doi.org/10.5194/acp-20-7595-2020>, 2020.

400 Hodzic, A., Jimenez, J. L., Madronich, S., Canagaratna, M. R., DeCarlo, P. F., Kleinman, L.,
401 and Fast, J.: Modeling organic aerosols in a megacity: potential contribution of semi-
402 volatile and intermediate volatility primary organic compounds to secondary organic
403 aerosol formation. *Atmos. Chem. Phys.*, 10, 5491-5514, [https://doi.org/10.5194/acp-10-](https://doi.org/10.5194/acp-10-5491-2010)
404 [5491-2010](https://doi.org/10.5194/acp-10-5491-2010), 2010.



- 405 Huang, C., Hu, Q. Y., Li, Y. J., Tian, J. J., Ma, Y. G., Zhao, Y. L., Feng, J. L., An, J. Y., Qiao, L.
406 P., Wang, H. L., Jing, S. A., Huang, D. D., Lou, S. R., Zhou, M., Zhu, S. H., Tao, S. K.,
407 and Li, L.: Intermediate volatility organic compound emissions from a large cargo vessel
408 operated under real-world conditions. *Environ. Sci. Technol.*, 52, 12934-12942,
409 <https://doi.org/10.1021/acs.est.8b04418>, 2018.
- 410 Huang, L., Wang, Q., Wang, Y. J., Emery, C., Zhu, A. S., Zhu, Y. H., Yin, S. J., Yarwood, G.,
411 Zhang, K., and Li, L.: Simulation of secondary organic aerosol over the Yangtze River
412 Delta region: the impacts from the emissions of intermediate volatility organic compounds
413 and the SOA modeling framework. *Atmos. Environ.*, 118079,
414 <https://doi.org/10.1016/j.atmosenv.2020.118079>, 2020.
- 415 Ho, K. F., Ho, S. S. H., Cheng, Y., Lee, S. C., and Yu, J. Z.: Real-world emission factors of
416 fifteen carbonyl compounds measured in a Hong Kong tunnel. *Atmos. Environ.*, 41, 1747-
417 1758, <https://doi.org/10.1016/j.atmosenv.2006.10.027>, 2007.
- 418 Jathar, S. H., Gordon, T. D., Hennigan, C. J., Pye, H. O., Pouliot, G., Adams, P. J., Donahue, N.
419 M., and Robinson, A. L.: Unspeciated organic emissions from combustion sources and
420 their influence on the secondary organic aerosol budget in the United States. *Proc. Natl.*
421 *Acad. Sci. U.S.A.*, 111, 10473-10478, <https://doi.org/10.1073/pnas.1323740111>, 2014.
- 422 Jimenez, J. L., Canagaratna, M. R., Donahue, N. M., Prevot, A. S. H., Zhang, Q., Kroll, J. H.,
423 DeCarlo, P. F., Allan, J. D., Coe, H., Ng, N. L., Aiken, A. C., Docherty, K. S., Ulbrich, I.
424 M., Grieshop, A. P., Robinson, A. L., Duplissy, J., Smith, J. D., Wilson, K. R., Lanz, V. A.,
425 Hueglin, C., Sun, Y. L., Tian, J., Laaksonen, A., Raatikainen, T., Rautiainen, J.,
426 Vaattovaara, P., Ehn, M., Kulmala, M., Tomlinson, J. M., Collins, D. R., Cubison, M. J.,



- 427 Dunlea, E. J., Huffman, J. A., Onasch, T. B., Alfarra, M. R., Williams, P. I., Bower, K.,
428 Kondo, Y., Schneider, J., Drewnick, F., Borrmann, S., Weimer, S., Demerjian, K., Salcedo,
429 D., Cottrell, L., Griffin, R., Takami, A., Miyoshi, T., Hatakeyama, S., Shimono, A., Sun,
430 J. Y., Zhang, Y. M., Dzepina, K., Kimmel, J. R., Sueper, D., Jayne, J. T., Herndon, S. C.,
431 Trimborn, A. M., Williams, L. R., Wood, E. C., Middlebrook, A. M., Kolb, C. E.,
432 Baltensperger, U., and Worsnop, D. R.: Evolution of organic aerosols in the atmosphere.
433 *Science*, 326, 1525–1529, <https://doi.org/10.1126/science.1180353>, 2009.
- 434 Kramer, L. J., Crilley, L. R., Adams, T. J., Ball, S. M., Pope, F. D., and Bloss, W. J.: Nitrous
435 acid (HONO) emissions under real-world driving conditions from vehicles in a UK road
436 tunnel. *Atmos. Chem. Phys.*, 20, 5231-5248, <https://doi.org/10.5194/acp-20-5231-2020>,
437 2020.
- 438 Li, S., Zhu, M., Yang, W. Q., Tang, M. J., Huang, X. L., Yu, Y. G., Fang, H., Yu, X., Yu, Q. Q.,
439 Fu, X. X.; Song, W., Zhang, Y. L., Bi, X. H., and Wang, X. M.: Filter-based measurement
440 of light absorption by brown carbon in PM_{2.5} in a megacity in South China. *Sci. Total*
441 *Environ.*, 633, 1360-1369, <https://doi.org/10.1016/j.scitotenv.2018.03.235>, 2018.
- 442 Liu, H., Man, H. Y., Cui, H. Y., Wang, Y. J., Deng, F. Y., Wang, Y., Yang, X. F., Xiao, Q., Zhang,
443 Q., Ding, Y., and He, K. B.: An updated emission inventory of vehicular VOCs and IVOCs
444 in China. *Atmos. Chem. Phys.*, 17, 12709-12724, [https://doi.org/10.5194/acp-17-12709-](https://doi.org/10.5194/acp-17-12709-2017)
445 2017, 2017.
- 446 Liu, T. Y., Wang, X. M., Wang, B. G., Ding, X., Deng, W., Lü, S. J., and Zhang, Y. L.: Emission
447 factor of ammonia (NH₃) from on-road vehicles in China: tunnel tests in urban Guangzhou.
448 *Environ. Res. Lett.*, 9, 064027, <https://doi.org/10.1088/1748-9326/9/6/064027>, 2014.



- 449 Liu, T. Y., Wang, X. M., Deng, W., Hu, Q. H., Ding, X., Zhang, Y. L., He, Q. F., Zhang, Z., Lü,
450 S. J., Bi, X. H., Chen, J. M., and Yu, J. Z.: Secondary organic aerosol formation from
451 photochemical aging of light-duty gasoline vehicle exhausts in a smog chamber. *Atmos.*
452 *Chem. Phys.*, 15, 9049-9062, <https://doi.org/10.5194/acp-15-9049-2015>, 2015.
- 453 Lu, Q., Murphy, B. N., Qin, M., Adams, P. J., Zhao, Y. L., Pye, H. O. T., Efstathiou, C., Allen,
454 C., and Robinson, A. L.: Simulation of organic aerosol formation during the CalNex study:
455 updated mobile emissions and secondary organic aerosol parameterization for
456 intermediate-volatility organic compounds. *Atmos. Chem. Phys.*, 20, 4313-4332,
457 <https://doi.org/10.5194/acp-20-4313-2020>, 2020.
- 458 Lu, Q., Zhao, Y. L., and Robinson, A. L.: Comprehensive organic emission profiles for gasoline,
459 diesel and gas-turbine engines including intermediate and semi-volatile organic compound
460 emissions. *Atmos. Chem. Phys.*, 18, 17637-17654, [https://doi.org/10.5194/acp-18-17637-](https://doi.org/10.5194/acp-18-17637-2018)
461 2018, 2018.
- 462 Murphy, B. N., Woody, M. C., Jimenez, J. L., Carlton, A. M. G., and Pye, H. O. T.: Semivolatile
463 POA and parameterized total combustion SOA in CMAQv5.2: impacts on source strength
464 and partitioning, *Atmos. Chem. Phys.*, 17, 11107-11133, [https://doi.org/10.5194/acp-17-](https://doi.org/10.5194/acp-17-11107-2017)
465 11107-2017, 2017.
- 466 Ots, R., Young, D. E., Vieno, M.; Xu, L., Dunmore, R. E., Allan, J. D., Coe, H., Williams, L.
467 R., Herndon, S. C., and Ng, N. L.: Simulating secondary organic aerosol from missing
468 diesel-related intermediate-volatility organic compound emissions during the clean air for
469 London (ClearfLo) campaign. *Atmos. Chem. Phys.*, 16, 1-36, [https://doi.org/10.5194/acp-](https://doi.org/10.5194/acp-16-6453-2016)
470 16-6453-2016, 2016.



- 471 Pye, H. O. T., and Seinfeld, J. H.: A global perspective on aerosol from low-volatility organic
472 compounds. *Atmos. Chem. Phys.*, 10, 4377–4401, [https://doi.org/10.5194/acp-10-4377-](https://doi.org/10.5194/acp-10-4377-2010)
473 2010, 2010.
- 474 Pierson, W. R., and Brachaczek, W. W.: Emissions of ammonia and amines from vehicles in the
475 road. *Environ. Sci. Technol.*, 17, 757-760, <https://doi.org/10.1021/es00118a013>, 1983.
- 476 Presto, A. A., and Miracolo, M. A.: Secondary organic aerosol formation from high-NO_x photo-
477 oxidation of low volatility precursors:n-alkanes. *Environ. Sci. Technol.*, 44, 2029-2034,
478 <https://doi.org/10.1021/es903712r>, 2010.
- 479 Qi, L. J., Liu, H., Shen, X. E., Fu, M. L., Huang, F. F., Man, H. Y., Deng, F. Y., Shaikh, A. A.,
480 Wang, X. T., Dong, R., Song, C., and He, K. B.: Intermediate-volatility organic compound
481 emissions from nonroad construction machinery under different operation modes. *Environ.*
482 *Sci. Technol.*, 53, 13832-13840, <https://doi.org/10.1021/acs.est.9b01316>, 2019.
- 483 Robinson, A. L., Donahue, N. M., Shrivastava, M. K., Weitkamp, E. A., Sage, A. M., Grieshop,
484 A. P., Lane, T. E., Pierce, J. R., and Pandis, S. N.: Rethinking organic aerosols: semivolatile
485 emissions and photochemical aging. *Science*, 315, 1259-1262,
486 <https://doi.org/10.1126/science.1133061>, 2007.
- 487 Shrivastava, M. K., Lane, T. E., Donahue, N. M., Pandis, S. N., and Robinson, A. L.: Effects of
488 gas particle partitioning and aging of primary emissions on urban and regional organic
489 aerosol concentrations. *J. Geophys. Res. Atmos.*, 113, D18301, [https://doi.org/](https://doi.org/10.1029/2007jd009735)
490 10.1029/2007jd009735, 2008.
- 491 Stewart, G. J., Nelson, B. S., Acton, W. J. F., Vaughan, A. R., Farren, N. J., Hopkins, J. R., Ward,
492 M. W., Swift, S. J., Arya, R., Mondal, A., Jangirh, R., Ahlawat, S., Yadav, L., Sharma, S.



- 493 K., Yunus, S. S. M., Hewitt, C. N., Nemitz, E., Mullinger, N., Gadi, R., Sahu, L. K.,
494 Tripathi, N., Rickard, A. R., Lee, J. D., Mandal, T. K., and Hamilton, J. F.: Emissions of
495 intermediate-volatility and semi-volatile organic compounds from domestic fuels used in
496 Delhi, India. *Atmos. Chem. Phys.*, 21, 2407-2426, [https://doi.org/10.5194/acp-21-2407-](https://doi.org/10.5194/acp-21-2407-2021)
497 2021, 2021.
- 498 Tang, R. Z., Lu, Q. Y., Guo, S., Wang, H., Song, K., Yu, Y., Tan, R., Liu, K. F., Shen, R. Z.,
499 Chen, S. Y., Zeng, L. M., Jorga, S. D., Zhang, Z., Zhang, W. B., Shuai, S. J., and Robinson,
500 A. L.: Measurement report: distinct emissions and volatility distribution of intermediate
501 volatility organic compounds from on-road chinese gasoline vehicle: implication of high
502 secondary organic aerosol formation potential. *Atmos. Chem. Phys.*, 21, 2569-2583,
503 <https://doi.org/10.5194/acp-21-2569-2021>, 2021.
- 504 Tkacik, D. S., Lambe, A. T., Jathar, S., Li, X., Presto, A. A., Zhao, Y. L., Blake, D., Meinardi,
505 S., Jayne, J. T., Croteau, P. L., and Robinson, A. L.: Secondary organic aerosol formation
506 from in-use motor vehicle emissions using a potential aerosol mass reactor. *Environ. Sci.*
507 *Technol.*, 48, 11235-11242, <https://doi.org/10.1021/es502239v>, 2014.
- 508 Wang, Y. H., Gao, W. K., Wang, S., Song, T., Gong, Z. Y., Ji, D. S., Wang, L. L., Liu, Z. R.,
509 Tang, G. Q., Huo, Y. F., Tian, S. L., Li, J. Y., Li, M. G., Yang, Y., Chu, B. W., Petaja, T. K.,
510 Kerminen, V.-M., He, H., Hao, J. M., Kulmala, M., Wang, Y. S., and Zhang, Y. H.:
511 Contrasting trends of PM_{2.5} and surface-ozone concentrations in China from 2013 to 2017.
512 *Nat. Sci. Rev.*, 7, 1331-1339, <https://doi.org/10.1093/nsr/nwaa032>, 2020.
- 513 Wu, L. Q., Wang, X. M., Lu, S. H., Shao, M., and Ling, Z. H: Emission inventory of semi-
514 volatile and intermediate-volatility organic compounds and their effects on secondary



- 515 organic aerosol over the Pearl River Delta region, *Atmos. Chem. Phys.*, 19, 8141-8161,
516 <https://doi.org/10.5194/acp-19-8141-2019>, 2019.
- 517 Wu, Y., Zhang, S. J., Hao, J. M., Liu, H., Wu, X. M., Hu, J. N., Walsh, M. P., Wallington, T. J.,
518 Zhang, M. K., and Stevanovic, S.: On-road vehicle emissions and their control in China:
519 a review and outlook. *Sci. Total Environ.*, 574, 332-349,
520 <https://doi.org/10.1016/j.scitotenv.2016.09.040>, 2017.
- 521 Yang, W. Y., Li, J., Wang, W. G., Li, J. L., Ge, M. F., Sun, Y. L., Chen, X. S., Ge, B. Z., Tong,
522 S. R., Wang, Q. Q., and Wang, Z. F.: Investigating secondary organic aerosol formation
523 pathways in China during 2014. *Atmos. Environ.*, 213, 133-147,
524 <https://doi.org/10.1016/j.atmosenv.2019.05.057>, 2019.
- 525 Zhang, Q., Jimenez, J. L., Canagaratna, M. R., Allan, J. D., Coe, H., Ulbrich, I., Alfarra, M. R.,
526 Takami, A., Middlebrook, A. M., and Sun, Y. L.: Ubiquity and dominance of oxygenated
527 species in organic aerosols in anthropogenically-influenced northern hemisphere
528 midlatitudes. *Geophys. Res. Lett.*, 34, L13801, <https://doi.org/10.1029/2007GL029979>,
529 2007.
- 530 Zhang, Y. L., Wang, X. M., Wen, S., Herrmann, H., Yang, W. Q., Huang, X. Y., Zhang, Z.,
531 Huang, Z. H., He, Q.F., and George, C.: On-road vehicle emissions of glyoxal and
532 methylglyoxal from tunnel tests in urban Guangzhou, China. *Atmos. Environ.*, 127, 55-60,
533 <https://doi.org/10.1016/j.atmosenv.2015.12.017>, 2016.
- 534 Zhang, Y. L., Yang, W. Q., Huang, Z. H., Liu, D., Simpson, I., Blake, D. R., George, C., and
535 Wang, X. M.: Leakage rates of refrigerants CFC-12, HCFC-22, and HFC-134a from
536 operating mobile air conditioning systems in Guangzhou, China: tests inside a busy urban



- 537 tunnel under hot and humid weather conditions. *Environ. Sci. Technol. Lett.*, 4, 481-486,
538 <https://doi.org/10.1021/acs.estlett.7b00445>, 2017.
- 539 Zhang, Y. L., Yang, W. Q., Simpson, I., Huang, X. Y., Yu, J. Z., Huang, Z. H., Wang, Z. Y.,
540 Zhang, Z., Liu, D., Huang, Z. Z., Wang, Y. J., Pei, C. L., Shao, M., Blake, D. R., Zheng, J.
541 Y., Huang, Z. J., and Wang, X. M.: Decadal changes in emissions of volatile organic
542 compounds (VOCs) from on-road vehicles with intensified automobile pollution control:
543 case study in a busy urban tunnel in South China. *Environ. Pollut.*, 233, 806-819,
544 <https://doi.org/10.1016/j.envpol.2017.10.133>, 2018.
- 545 Zhang, Y. L., Deng, W., Hu, Q. H., Wu, Z. F., Yang, W. Q., Zhang, H. N., Wang, Z. Y., Fang,
546 Z., Zhu, M., Li, S., Song, W., Ding, X., and Wang, X. M.: Comparison between idling and
547 cruising gasoline vehicles in primary emissions and secondary organic aerosol formation
548 during photochemical ageing. *Sci. Total Environ.*, 772, 137934,
549 <https://doi.org/10.1016/j.scitotenv.2020.137934>, 2020.
- 550 Zhao, Y. L., Hennigan, C. J., May, A. A., Tkacik, D. S., de Gouw, J. A., Gilman, J. B., Kuster,
551 W. C., Borbon, A., and Robinson, A. L.: Intermediate-volatility organic compounds: a
552 large source of secondary organic aerosol. *Environ. Sci. Technol.*, 48, 13743-13750,
553 <https://doi.org/10.1021/es5035188>, 2014.
- 554 Zhao, Y. L., Nguyen, N. T., Presto, A. A., Hennigan, C. J., May, A. A., and Robinson, A. L.:
555 Intermediate volatility organic compound emissions from on-road diesel Vehicles:
556 chemical composition, emission factors, and estimated secondary organic aerosol
557 production. *Environ. Sci. Technol.*, 49, 11516-11526,
558 <https://doi.org/10.1021/acs.est.5b02841>, 2015.



559 Zhao, Y. L., Nguyen, N. T., Presto, A. A., Hennigan, C. J., May, A. A., and Robinson, A. L.:
560 Intermediate volatility organic compound emissions from on-road gasoline vehicles and
561 small off-road gasoline engines. Environ. Sci. Technol., 50, 4554-4563,
562 <https://doi.org/10.1021/acs.est.5b06247>, 2016.
563



564 **Figure captions**

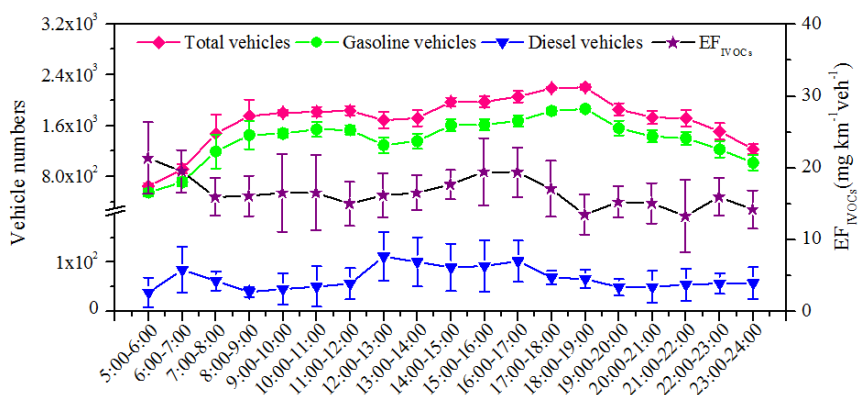
565 Figure 1. Diurnal variations of vehicle fleets and fleet-average EF_{IVOCs} during the sampling
566 period. Error bars represent 95% confidence intervals.

567 Figure 2. Comparison of the EF_{IVOCs} measured in this study with that previously measured for
568 fossil fuel combustion sources. The error bars in (a) represent 95% confidence
569 interval. In (b), the boxes represent the 75th and 25th percentiles, the centerlines are
570 the medians and squares are the averages. The whiskers represent 10th and 90th
571 percentiles. SORMs refer to small off-road engines fueled with gasoline. NRCMs
572 represent non-road construction machineries fueled with diesel.

573 Figure 3. The average emission factor of vehicular IVOCs in different bins measured during
574 the campaign.

575 Figure 4. The predicted SOA formation potentials from different classes of precursors (VOC
576 and IVOCs). The error bars represent 95% confidence intervals.

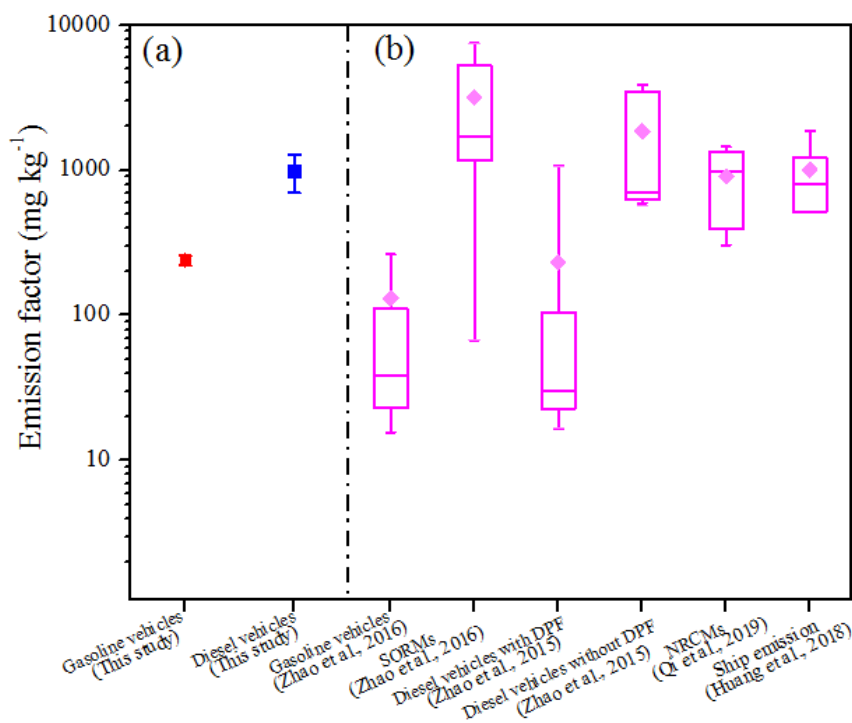
577



578

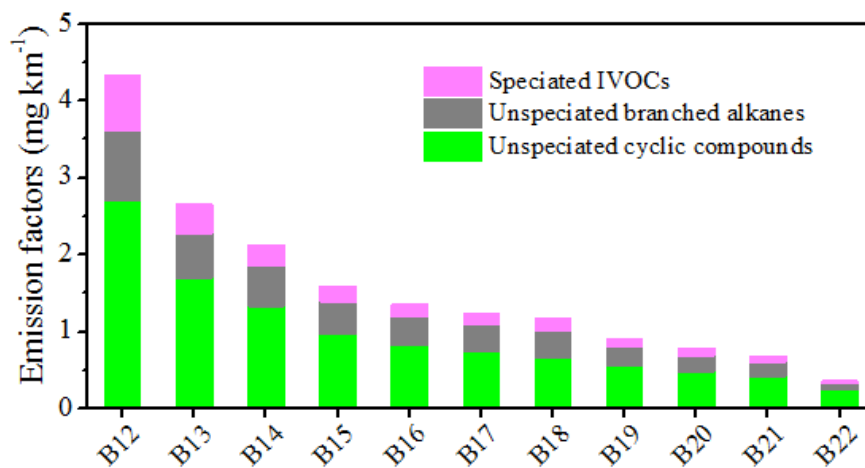
579 Figure 1. Diurnal variations of vehicle fleets and fleet-average EF_{IVOCs} during the sampling

580 period. Error bars represent 95% confidence intervals.



581

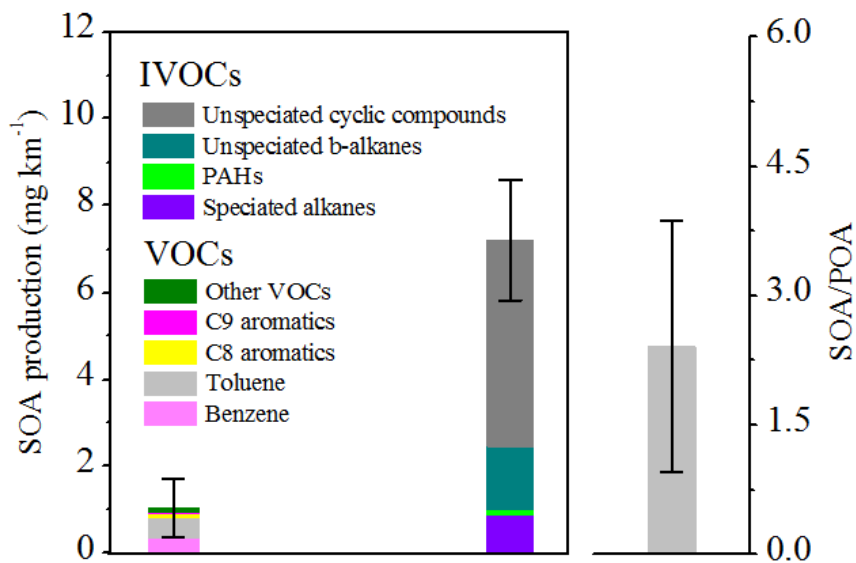
582 Figure 2. Comparison of the EF_{IVOCs} measured in this study with that previously measured for
583 fossil fuel combustion sources. The error bars in (a) represent 95% confidence interval. In (b),
584 the boxes represent the 75th and 25th percentiles, the centerlines are the medians and squares are
585 the averages. The whiskers represent 10th and 90th percentiles. SORMs refer to small off-road
586 engines fueled with gasoline. NRCMs represent non-road construction machineries fueled with
587 diesel.



588

589 Figure 3. The average emission factor of vehicular IVOCs in different bins measured during

590 the campaign.



591

592 Figure 4. The predicted SOA formation potentials from different classes of precursors (VOC

593 and IVOCs). The error bars represent 95% confidence intervals.